From $VO_2(B)$ to $VO_2(R)$: Theoretical structures of VO_2 polymorphs and *in situ* electron microscopy

Ch. Leroux and G. Nihoul
LMMI, University of Toulon-Var, BP 132, F-83957 La Garde Cedex, France

G. Van Tendeloo
EMAT, University of Antwerp (RUCA), Groenenborgerlaan 171, B-2020 Antwerp, Belgium

(Received 27 May 1997)

The intermediate steps of the phase transition between the metastable monoclinic $VO_2(B)$ phase and the stable tetragonal rutile $VO_2(R)$ phase have been studied by *in situ* electron microscopy. A crystallographic interpretation based on the static concentration waves theory is proposed: as temperature increases, the long-range order in the complex monoclinic $VO_2(B)$ phase is lost and gradually a first intermediate ill crystallized phase with a *drastically* reduced symmetry is formed as evidenced from the diffraction patterns. Next, a new tetragonal phase is generated that corresponds to a state where some of the vanadium atoms are now in a disordered state. When annealing inside the microscope, this phase grows out into a superstructure, with coexistence of two possible orientation variants. In all these phases the VO_6 octahedra remain virtually parallel, but for the final transition around 450 °C into the rutile stable phase, half of the octahedra have to reorient; the transition therefore has the aspects of a *reconstructive* one as is evident from the *in situ* experiment. [S0163-1829(98)05505-2]

I. INTRODUCTION

Vanadium dioxide can adopt different structures. The most stable is the rutile one which, when heated at 68 °C, shows a reversible metal-insulator phase transition $VO_2(M) \leftrightarrow VO_2(R)$ associated with drastic changes in the optical properties such as a rapid decrease in optical transmittance in the near-IR region. Recently, thermochromic pigment of VO_2 has been used in a polymer composite coating.[1] In order to obtain good coatings, the use of submicrometer powders of $VO_2(R)$ is indispensable: the original method used in Ref. 1 to produce submicron thermochromic VO_2 powders involves an intermediate reduction step in which the $VO_2(B)$ metastable allotropic phase is formed. The thermal decomposition of ammonium hexavanadate at 600 °C followed by pyrolysis at low temperature (<380 °C), produces metastable $VO_2(B)$: the transformation of this black, or bluish, nonthermochromic powder into rutile VO_2 is a crucial step for the final morphology that influences the optical properties.

Transformations between the different polymorphs of VO_2 were reported in the literature. Concerning the transformation with increasing temperature of $VO_2(B)$ into $VO_2(R)$, Theobald reported the sequence $VO_2(B) \rightarrow VO_2(A) \rightarrow VO_2(R)$,[3] which was realized by hydrothermal treatment. The $VO_2(A)$ phase is metastable and has a tetragonal structure. However, Theobald specified that he did not observe the occurrence of $VO_2(A)$ when starting from $VO_2(B)$ under normal pressure.[3] It seems that, starting from $VO_2(B)$, this $VO_2(A)$ phase can only be obtained under particular pressure conditions (hydrothermal treatment of the $VO_2(B)$ phase). Oka, Yao, and Yamamoto confirmed the importance of pressure conditions in the growth of the $VO_2(A)$ phase, starting from $VO_2(B)$.[4] The crystallographic relationships between $VO_2(B)$ and $VO_2(A)$ were studied by Oka, Yao, and Yamamoto;[5] the unit cells of both phases are related $\mathbf{c}_A = 2\mathbf{b}_B$ and $\mathbf{a}_A \approx \mathbf{a}_B/2 + \mathbf{c}_B$, but it is quite obvious that the octahedra arrangement in both structures is very different. The transformation of $VO_2(B)$ in $VO_2(R)$ has also been studied recently by thermogravimetry and analysis and Fourier transform infrared spectroscopy methods[2] under normal pressure and it has been shown that the transformation occurs at least in two stages. It certainly is not a simple transformation occurring at a fixed temperature. In this work, we have followed the transformation by electron diffraction and electron microscopy: the production of $VO_2(R)$ by heating $VO_2(B)$ up to 450 °C under low-pressure conditions, as it occurs in the electron microscope, to our knowledge has not been reported before.

II. CRYSTALLOGRAPHY OF VANADIUM DIOXIDES

Generally speaking, the structures of the four VO_2 polymorphs, $VO_2(R)$, $VO_2(M)$, $VO_2(B)$, and $VO_2(A)$, are based on an oxygen bcc lattice with vanadium in the octahedral sites, the oxygen octahedra being more or less regular. They can be separated in two groups, depending on the mutual orientation of the fourfold axis of the oxygen octahedra. The oxygen octahedra can be aligned either along two perpendicular directions, as it is the case in rutile structure $VO_2(R)$, and in monoclinic deformed $VO_2(M)$; or oxygen octahedra can be mainly aligned along one direction as in $VO_2(B)$ and $VO_2(A)$. Note that these two groups correspond to two different values for the density (see Table I). It is clear that, although these VO_2 polymorphs correspond to the same stoichiometry, their structures are very different.

The most stable structure for vanadium dioxide is the so-called rutile structure $VO_2(R)$, which is stable from 68 °C to 1540 °C: the tetragonal cell has parameters $a = b = 4.55$ Å, $c = 2.88$ Å, $Z = 2$; the space group is $P4_2/mmm$ (136).[6,7] Atomic positions are listed in Table II. This group gives rise to a very symmetric structure; vanadium atoms are

TABLE I. Densities of VO_2 polymorphs.

	Density (g/cm^3)
$VO_2(R)$	4.67
$VO_2(M)$	4.67
$VO_2(B)$	4.031
$VO_2(A)$	4.035

at the center of regular oxygen octahedra (two V-O bonds at 0.1933 nm, the four others at 0.1922 nm), with their fourfold axes aligned alternatively along [110] and [1$\bar{1}$0] [see Fig. 1(a)]. The different octahedra share edges, building chains along the c axis of the structure [see Fig. 1(b)].

The formation at 68 °C of the monoclinic $VO_2(M)$ is related to the appearance of a pairing between two V^{4+} along $\mathbf{c}_R$. The induced distortion leads to a lowering of the symmetry. We obtain a monoclinic cell with cell parameters related to the rutile structure: $\mathbf{a}_M = 2\mathbf{c}_R$, $\mathbf{b}_M = \mathbf{a}_R$, $\mathbf{c}_M = \mathbf{b}_R - \mathbf{c}_R$. The cell parameters of the room temperature phase $VO_2(M)$ are $a = 5.75$ Å, $b = 5.42$ Å, $c = 5.38$ Å, $\beta = 122.6°$, $Z = 4$, the space group is $P2_1/c$ (14).[6,8,9] Atomic positions are listed in Table III.

In the $VO_2(M)$ structure, one has also a pattern of octahedra aligned along two perpendicular directions [see Fig. 2(a)], but the octahedra are no longer regular. There is now one short distance V-O (0.176 nm) corresponding to a double link. The vanadium atoms have shifted from the center of the octahedra [see Fig. 2(a)] and form chains that are no longer parallel to the c_R axis (i.e., a_M) [Fig. 2(b)]. There are now two different distances between vanadium atoms 0.2615 and 0.3162 nm instead of 0.2851 nm for the rutile structure, leading to a doubling of the cell along the c_R axis of the rutile phase.

The two other polymorphs of VO_2 have little in common with the rutile phase. They have larger cells, with octahedra mainly aligned along one crystallographic direction. A monoclinic structure was proposed by Théobald, Cabala, and Bernhard[10] for $VO_2(B)$ obtained by gentle reduction (hydrothermal treatment) of V_2O_5. The parameters of the monoclinic cell are: $a_B = 12.03$ Å, $b_B = 3.693$ Å, $c_B = 6.42$ Å, and $\beta = 106.6°$, $Z = 8$ and the space group is $C2/m$ (12). Atomic positions are listed in Table IV. The $VO_2(B)$ structure can be considered as formed by two identical layers of atoms along **b**. Figure 3 shows the arrangement of octahedra in the (010) plane of $VO_2(B)$: the second layer is shifted with respect to the first one by $\frac{1}{2}$, $\frac{1}{2}$, 0. In this structure, the oxygen octahedra are deformed, the vanadium atoms being no longer in their center; this leads to two types of octahedra. The ex-fourfold axes of the oxygen octahedra are more or less aligned along a single crystallographic direction,

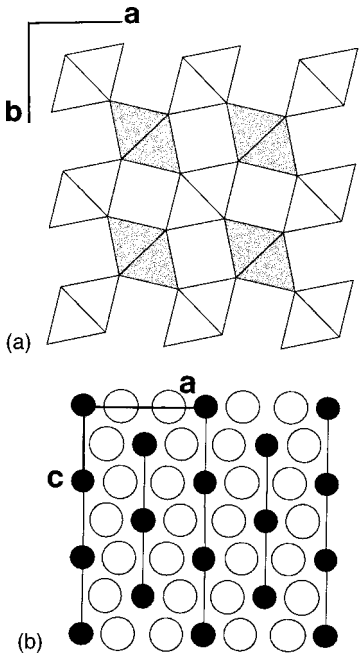

FIG. 1. (a) Projection of the rutile structure along [001], showing the two perpendicular orientations of the octahedra, drawn white for vadanium atoms at $z = 0$ and grey for vanadium atoms at $z = \frac{1}{2}$. (b) projection along [010]. Vanadium atoms built chains parallel to the **c** axis of the structure. Vanadium atoms are drawn black and oxygen atoms white.

namely, [010]. Striking similarities exist between the $VO_2(B)$ and the V_6O_{13} structure. These similarities were already noticed in Ref. 10. Like V_6O_{13}, $VO_2(B)$ forms platelets, their size depending on the preparation method. These platelets are preferentially oriented. They grow in (**a**,**b**) planes; this can be inderstood from Fig. 3 because in this plane one forms a network of corner sharing octahedra. $VO_2(B)$ and V_6O_{13} only differ in the way the octahedra are linked in the (**a**,**b**) plane; they exhibit a similar [001] diffraction pattern.

The other metastable phase of vanadium dioxyde called $VO_2(A)$ was first reported by Theobald,[3] as an intermediate phase in the transformation $VO_2(B) \rightarrow VO_2(R)$; it has been fully characterized by Oka *et al.* $VO_2(A)$ is tetragonal with cell parameters $a = b = 8.44$ Å, $c = 7.68$Å, $Z = 16$, space group $P42/nmc$ (138).[5] Atomic positions are listed in Table V. Figure 4 shows a projection along the [001] direction. Like in $VO_2(B)$, the fourfold axes of the oxygen octahedra are aligned along a single direction, in this case the **c** axis of the tetragonal structure. Note that this c parameter is roughly twice the b axis of $VO_2(B)$; the oxygen octahedra are less deformed than in $VO_2(B)$ and there is only one type of octahedron.

TABLE II. Atomic positions for $VO_2(R)$.

		x	y	z
V	$2a$	0	0	0
O	$4f$	0.305	0.305	0

TABLE III. Atomic positions for $VO_2(M)$.

		x	y	z
V	$4e$	0.242	0.975	0.025
O1	$4e$	0.1	0.21	0.20
O2	$4e$	0.39	0.69	0.29

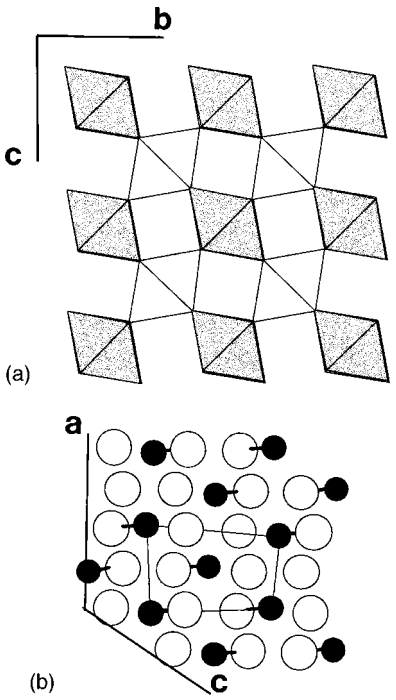

FIG. 2. Projection of the $VO_2(M)$ structure along [100] (ex-**c** axis of the rutile cell). (b) projection along [010]. The double liaison V-O is drawn as a heavy line. The ex-rutile cell is drawn as a grey line in order to emphasize the distortion between $VO_2(R)$ and $VO_2(M)$.

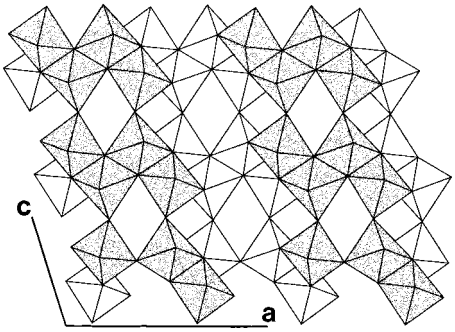

FIG. 3. Projection of the $VO_2(B)$ structure along [010]. For simplicity, the atoms are not represented. There are packing of edge sharing octahedra that are only linked by corners in (a,b) planes. Octahedra at $y=0$ and $y=\frac{1}{2}$ are, respectively, represented white and grey.

III. THEORETICAL DEDUCTION OF POSSIBLE STRUCTURES

A. General considerations

In order to study the transition from $VO_2(B)$ to $VO_2(R)$, we will unravel the structure of these two polymorphs. In both structures, the oxygens are distributed on a body-centered-cubic lattice and we will start from this oxygen lattice. *Unless otherwise stated, all notations will refer to the bcc lattice.* Vanadium atoms can be added to this lattice in octahedral sites. There are six possible octahedral sites for one bcc oxygen cell (two oxygen atoms). In a VO_2 compound, (one vanadium for two oxygens), $\frac{5}{6}$ of the octahedral sites will be empty and only $\frac{1}{6}$ site will be occupied. In a completely disordered phase vanadium atoms and their vacancies would be randomly distributed between the octahedral sites of the bcc host lattice. The elementary cell for a completely disordered phase would be the bcc lattice with slightly larger parameters and the resulting diffraction pattern would correspond to the reciprocal lattice of the bcc host lattice. The room-temperature diffraction patterns of $VO_2(B)$ or $VO_2(R)$ indeed exhibit strong reflections corresponding to the bcc positions. However, it is obvious that there are many supplementary spots, indicating that vanadium atoms and vacancies are ordered. This means that a high-temperature order-disorder phase transition is a possible scheme.

To deduce the ordered arrangements of the vacancies in the periodic structure, we will use the static concentration wave (SCW) method which, initially, was applied to describe ordering in substitutional-interstitial solid solutions and was then extended to the case of layer structures for some metal oxides by Khachaturyan and Pokrovskii.[11]

The main idea is that the ordered structures will have new periodicities, as compared to the disordered one, and that they can be described by a superposition of static concentration waves with wave vectors $\mathbf{k_j}$, corresponding to these new periodicities. The most stable structure will correspond to the minimum of the configuration energy. In an Ising model, we can define the interaction energy between two atoms, $W(R)$, and write it as a Fourier series on the SCW. This gives us the Fourier transform, $V(\mathbf{k_j})$, and its eigenvalues, $\lambda_w(\mathbf{k_j})$. It has been shown in Ref. 11, that the total configuration energy can then be written as a sum of these eigenvalues weighted by square modulus of the corresponding amplitudes. Then, to obtain the minimum energy, the amplitude of the SCW that corresponds to the minimum $\lambda_w(\mathbf{k_j})$ must be maximal: this SCW will be called the dominant wave and its wave vector will be called $\mathbf{k}_0$. This condition is the maximal amplitude principle, and we will use it further in our considerations.

As was shown by Khachaturyan and Pokrovskii,[11] the maximum amplitude principle is automatically fulfilled if the wave vectors of the ordered structure are equal to $\frac{1}{2}$, $\frac{1}{3}$, and $\frac{1}{4}$ of a fundamental reciprocal lattice vector **H** of the disordered crystal. However, in many layer structures, the wave vectors have arbitrary values, $\mathbf{H}/n$ with $n>4$, and then the

TABLE IV. Atomic positions for $VO_2(B)$.

		x	y	z
V1	4*i*	0.803	0	0.725
V2	4*i*	0.902	0	0.300
O1	4*i*	0.863	0	0.991
O2	4*i*	0.738	0	0.373
O3	4*i*	0.934	0	0.595
O4	4*i*	0.642	0	0.729

TABLE V. Atomic positions for $VO_2(A)$.

		x	y	z
V	16*j*	0.1894	0.0176	0.0118
O1	16*j*	0.1674	0.0012	0.3743
O2	8*i*	0.1634		0.3416
O3	8*i*	0.1352		0.8930

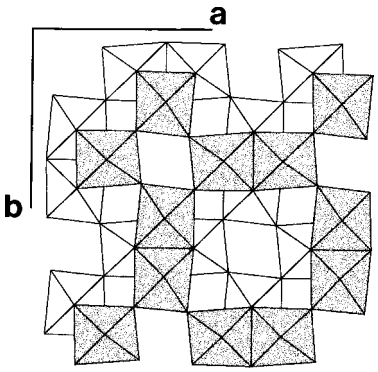

FIG. 4. Projection along [001] of the $VO_2(A)$ structure. The structure consists of four layers of oxygen octahedra perpendicular to **c**, respectively drawn white and grey.

dominant wave $\mathbf{k}_0$ should inevitably be supplemented with nondominant waves with wave vectors $\mathbf{k_s}=s\mathbf{k}_0$ where s is an integer and has a maximum value s_1, such that $\mathbf{k_s}$ is not a vector of the reciprocal disordered lattice as long as $s \leqslant s_1$. The stability of these structures decreases with increasing s_1 because, if we increase the number of nondominant waves, the configuration energy increases.

B. Ordering leading to $VO_2(R)$

We start from the bcc oxygen lattice. Following Pokrovskii and Kachaturyan[12] we divide the possible octahedral sites in three sublattices obtained by three different translations from a given oxygen position: $[\frac{1}{2},0,0]$ (O_x sublattice), $[0,\frac{1}{2},0]$ (O_y sublattice), and $[0,0,\frac{1}{2}]$ (O_z sublattice); each sublattice has two possible sites for the vanadium atoms. The SCW theory allows us to estimate the change in energy induced by the possible ordering of vacancies; if the ordering decreases the energy, the ordered structure can be stable. It is clear that this theory cannot incorporate small structural deformations, induced by the appearance of interstitials and vacancies.

Pokrovskii and Kachaturyan[12] have shown that the first ordering that can diminish the energy of the vanadium atoms is obtained for a dominant wave $\mathbf{k}_0=0$ (and no nondominant waves): (a) either if only one octahedral sublattice is filled (e.g., O_z); (b) or if only two sublattices are filled (e.g., O_x and O_y), the last one (O_z) being vacant. For both cases, the wave vector is $\mathbf{k}_0=0$ so that no new reflections appear: the diffraction patterns will be unmodified.

The last possibility, where we keep two types of octahedral sublattices, has two ordered vacancies on the O_z octahedral sublattice, which leaves us with three vacancies and one vanadium atom that are still disordered but have to be on the O_x and O_y sublattices. From this basic structure, two successive orderings (with $\mathbf{k}_0=\frac{1}{2},-\frac{1}{2},0$ and $\mathbf{k}_0=\frac{1}{2},\frac{1}{2},0$) lead Pokrovskii and Kachaturyan[13] to the rutile structure. Note that all ordering schemes were obtained with only dominant waves so that the resulting structure will be stable. Taking into account the presence of vacancies and vanadium atoms on the three possible sublattices, the rutile VO_2 should be written as $(V_{1/4}\square_{3/4})_x(V_{1/4}\square_{3/4})_y(\square)_zO$ where $\square$ stands for a vacancy.

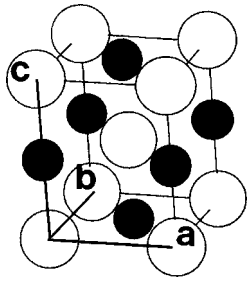

FIG. 5. Tetragonal cell obtained when one sublattice (O_z) is occupied by vanadium atoms.

C. Initial ordering for $VO_2(B)$

$VO_2(B)$ differs in many points from the rutile VO_2.

(a) Though the oxygen octahedra are deformed, we can still define their fourfold axes. In the case of $VO_2(B)$ these axes are all parallel while for $VO_2(R)$ they are along two perpendicular directions as explained before.

(b) The structure is very irregular, with condensed parts and less condensed parts. It is rather like the homologous series structures V_nO_{2n-1}, where the vanadium atoms have different valences, though, in $VO_2(B)$, all vanadium atoms have a valency 4.

(c) As already mentioned, the $VO_2(B)$ structure is looser: this is macroscopically measured by a lower density. Moreover, the bcc oxygen lattice in $VO_2(B)$ has one vacancy for eight occupied sites, while, in the rutile form, the bcc oxygen lattice is fully occupied.

These data about $VO_2(B)$ suggested us to start from the idea to have only *one* octahedral sublattice filled (a possibility proposed by Pokrovskii and Kachaturyan[12]). We then have four ordered vacancies on two of the octahedral sublattices O_x and O_y, which will remain empty in all the successive possible orderings. There is only one vacancy and one vanadium atom left that can occupy the two sites of the O_z octahedral sublattice. As a consequence, the **c** axis will be elongated (Fig. 5) and the cell is now tetragonal rather than cubic. If the c axis reaches the value of $a\sqrt{2}$ the centered tetragonal cell can be rewritten as a face-centered-cubic cell. Indeed, the oxide VO exists and has a NaCl structure; its parameter is 0.406 nm, which would give a parameter $a \approx 0.29$ nm for our starting bcc cell. In VO, however, the vanadium appears as V^{2+} [$2R(O^{2-})+2R(V^{2+}) \approx 0.44$ nm] while in $VO_2(B)$ it appears as V^{4+}, which implies a smaller ionic radius. Indeed, the fourfold axes of the octahedra in $VO_2(B)$ have a length equal to 0.369 nm to be compared with $2R(O^{2-})+2R(V^{4+})$, which is ≈ 0.39 nm.

To better understand our starting structure, we first draw the ''ideal'' $VO_2(B)$, i.e., we put all the atoms (vanadium or oxygen) on the exact sites they would occupy in the undistorted bcc lattice. SCW theory will never produce these small displacements anyway. The resulting structure is depicted in Fig. 6 and the two main corresponding diffraction patterns appear in Fig. 7. The oxygen atoms form a centered lattice that is tetragonal rather than cubic, with cell dimensions 0.29 and 0.37 nm. The monoclinic $VO_2(B)$ and the initial body-centered lattices are related in the following way:

$$\mathbf{a}_B=3\mathbf{a}+3\mathbf{b}, \quad \mathbf{a}_B^*=1/9(2\mathbf{a}^*+\mathbf{b}^*),$$

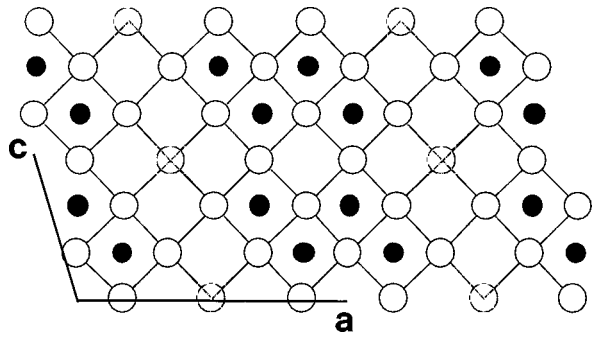

FIG. 6. One (010) plane for the idealized $VO_2(B)$ structure. Vanadium atoms are drawn black and oxygen atoms white. Note that, with respect to the perfect oxygen bcc lattice, there are oxygen vacancies, drawn here with dotted lines.

$$\mathbf{b}_B=\mathbf{c},\quad \mathbf{b}_B^*=\mathbf{c}^*,$$

$$\mathbf{c}_B=\mathbf{a}-2\mathbf{b},\quad \mathbf{c}_B^*=1/3(\mathbf{a}^*-\mathbf{b}^*).$$

The correspondence between some planes and directions in both systems is given in Table VI. If we take into account the intensities of the different structure factors, we see that all the reflexions that do not correspond to a bcc reciprocal lattice can be generated from only two additional waves, the $\frac{1}{3}(1,-1,0)$ $[(001)_B]$ and the $\frac{1}{9}(2,1,9)$ $[(110)_B]$. We therefore have two possibilities for calculating the $VO_2(B)$ structure: either start from the structural data given above to choose the waves that are introduced as compared to the oxygen bcc lattice or calculate and minimize an evaluation of the vanadium system energy.

The result of this first ordering of vacancies that will be the start for the further orderings can be written as $(\square)_x(\square)_y$ (disordered $V_{1/2}\square_{1/2})_zO$.

D. Further orderings for $VO_2(B)$: from structural data

We have two independent superstructure waves that appear in the diffraction pattern of $VO_2(B)$ as compared to the bcc lattice. Hence, we need two different successive orderings to reach $VO_2(B)$.

We start from a disordered situation (see before) where all sites are occupied by $(V_{1/2}\,\square_{1/2})$ and we want to reach an ordered structure where one half of the sites are fully occupied by vanadium atoms (and $\frac{1}{2}$ are vacant). The SCW $\frac{1}{3}(1,-1,0)$ can only order $\frac{1}{3}$ (or $\frac{2}{3}$) of the vacancies leaving $\frac{2}{3}$ (or $\frac{1}{3}$) possible sites for vanadiums. The SCW $\frac{1}{9}(2,1,9)$ can order a fraction $n/9$ of vacancies, where n is an integer, leaving $(9-n)/9$ sites for vanadiums. The resulting number of ordered vanadiums will be $\frac{2}{3}$ (or $\frac{1}{3}$) multiplied by $(9-n)/9$ and has to be $\frac{1}{2}$ (or very near it). The only solution is $n=3$ giving the final formula $(\square)_x(\square)_y(V_{4/9}\,\square_{5/9})_zO$.

Starting ordering the bcc lattice with the SCW $\frac{1}{9}(2,1,9)$ as a dominant wave implies that we must also have nondominant waves. The ordering induced by this SCW is given by the so-called clock diagram (Fig. 8) where we order three vacancies planes. It leads to the following sequence of (2,1,9) planes $\square\square\square\times\times\times\times\times\times\square\square\square\times\times\times\times\times\times$ where $\times$ stands for planes that can be occupied by vanadiums and vacancies while $\square$ stands for a completely empty plane. The resulting structure is shown in Fig. 9(a). The second ordering is applied on the remaining possible sites for vanadiums (planes marked $\times$) and is given by the dominant wave $\frac{1}{3}(1,-1,0)$. The corresponding occupation probability is then

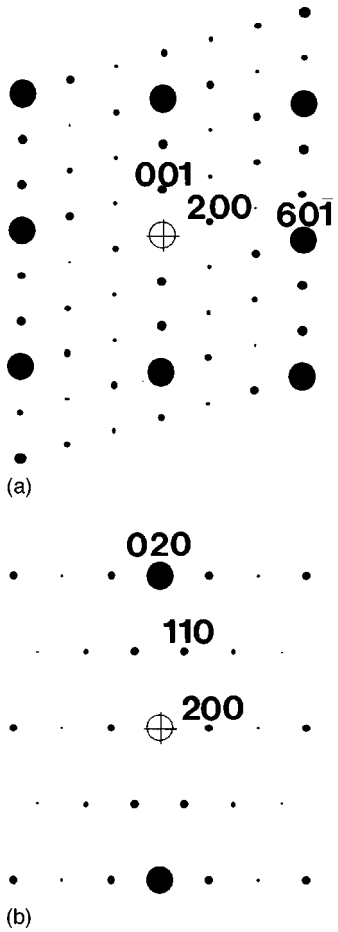

FIG. 7. Kinematical calculated diffraction patterns for the ''ideal'' $VO_2(B)$ corresponding to (a) $[010]_B$ and (b) $[001]_B$ zone axes.

$$n(x,y,z)=\tfrac{2}{3}-\tfrac{2}{3}\cos[2\pi(x-y)/3].$$

This means vacancies will be located on every third $(1,-1,0)$ plane, when $x-y=3p$ where p is an integer $[n(x,y,z)$ is then equal to 0]. The corresponding structure is shown in Fig. 9(b) and would correspond to a formula $(V_{4/9}\square_{5/9})$ O or V_4O_9. We remark that an equivalent ordering would have been obtained with the dominant wave $\frac{1}{3}(2,1,3)$: this is obvious in real space [Fig. 9(b)] but can also be understood because the two waves are equivalent

TABLE VI. Correspondence between planes and directions in the monoclinic and bcc lattices of $VO_2(B)$.

$VO_2(B)$ Monoclinic cell	bcc cell
(0,2,0)	(0,0,2)
(1,1,0)	1/9(2,1,9)
(0,0,1)	1/3(1,−1,0)
[1 0 6]	[1 −1 0]
[0 0 1]	[1 −2 0]

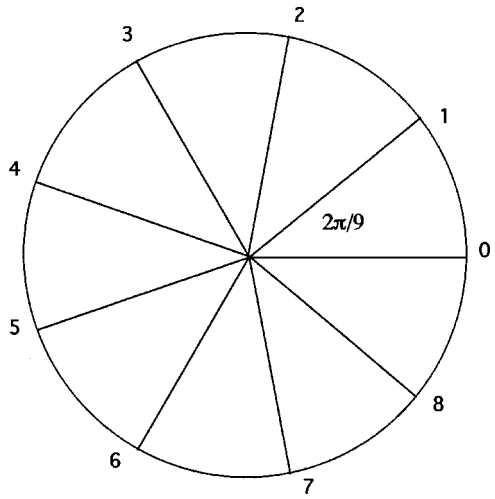

FIG. 8. Clock diagram for the SCW $\frac{1}{9}$ (2,1,9). One has simply to find the sequence of vacant planes that gives the maximum amplitude. In this case, it is three consecutive planes.

$\{(\frac{2}{3},\frac{1}{3},\frac{3}{3})=(1,0,1)-(\frac{1}{3},-\frac{1}{3},0)\}$. This remark is interesting as it shows that the $VO_2(B)$ structure is obtained by two successive orderings along two families of planes parallel to the c_B axis.

This heterogeneous distribution, however, will obviously induce unequal chemical potential values for different oxygen atoms. Such a system cannot be stable. This nonequilibrium situation is usually changed by introducing small displacements of atoms and/or by the creation of vacancies in the host lattice. In our case, we can see that one oxygen atom [marked by an arrow on Fig. 9(b)] is only loosely linked to the vanadium atoms as it does not belong to any octahedron. An oxygen vacancy will be very easily formed on that site and one obtains a VO_2 composition for our compound. Only slight rearrangements are now needed to obtain $VO_2(B)$.

The structure can be described as consisting of groups of filled (2,1,9) planes separated by groups of vacant planes. The groups are linked by identical but translated groups in the upper and lower planes perpendicular to **c**.

E. Further orderings for $VO_2(B)$: by minimization of the energy

We start again from the $(\square)_x(\square)_y$ (disordered $V_{1/2}\square_{1/2})_zO$ structure. Following the SCW theory, we calculate the Fourier transform W of the energy of this tetragonal system. Vanadium atoms have eight nearest neighbors at a distance of $(a^2/2+c^2/4)^{1/2}$, four atoms at a, two at a distance of c and four at $a\sqrt{2}$. We have taken into account the fact that, now, the c axis has a parameter larger than the a (or b) parameter but that it is probably less than $a\sqrt{2}$ (see earlier). We obtain for W:

$$W=8X_1\cos\pi k_x\cos\pi k_y\cos\pi k_z+2X_2(\cos2\pi k_x+\cos2\pi k_z)$$
$$+2X_3\cos2\pi k_y+4X_4\cos2\pi k_x\cos2\pi k_z,$$

where X_1, X_2, X_3, and X_4 are constants for the interactions with the first, second, third, and fourth neighbors: $X_1>X_2>X_3>X_4>0$. k_x, k_y, and k_z are the components of a reciprocal vector **k**, which characterizes the concentration wave generated by the ordering. The minimum energies are easy to obtain when only one dominant wave is present,[13] this corresponds to a vector **k** equal to a bcc reciprocal vector **H**, divided by 2, 3, or 4. In the first Brillouin zone, all the possibilities are in the stars listed herein: **H**/2:{000}, {100}, $\{\frac{1}{2}\ \frac{1}{2}0\}$; **H**/3:$\{\frac{2}{3}\ 0\ 0\}$ $\{\frac{1}{3}\ \frac{1}{3}0\}$, $\{\frac{2}{3}\ \frac{2}{3}\}$; **H**/4:$\{\frac{1}{2}\ \frac{1}{2}\ \frac{1}{2}\}$, $\{\frac{1}{4}\ \frac{1}{4}0\}$, $\{\frac{1}{2}00\}$.

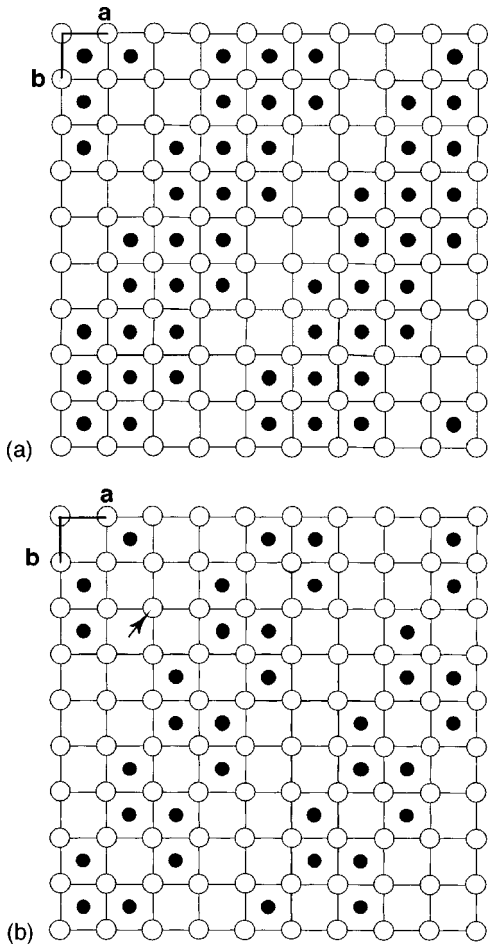

FIG. 9. (a) One plane ($z=0$) in the new cell (9**a**, 9**b**, **c**) showing the ordering of vacancies corresponding to packing of three sequential $\frac{1}{9}$ (2,1,9) planes. (b) The same plane $z=0$ after a second ordering of vacancies where one (1,−1,0) plane over three is empty.

The minimum energy is obtained for the star $\{\frac{2}{3}\ \frac{2}{3}\ \frac{2}{3}\}$; among the members of this star, we can choose whichever wave seems more suitable for our description as all the waves in the star will give rise to the same structure. The value of W is the same for all members of the star and is $W(\frac{2}{3},\frac{2}{3},\frac{2}{3})=-X_1-2X_2-X_3+X_4$; this corresponds to a large decrease in energy. Remembering the results obtained in the previous paragraph, we choose either $\mathbf{k}_1=\frac{1}{3}$ (2,1,1) or $\mathbf{k}_1'=\frac{1}{3}$ (1,−1,2) as the dominant wave. The corresponding occupation probabilities of the sites in the only remaining octahedral sublattice O_z are

$$n(x,y,z)=\tfrac{2}{3}-\tfrac{2}{3}\cos[2\pi(x-y+2z)/3]$$
$$=\tfrac{2}{3}-\tfrac{2}{3}\cos[2\pi+y+z)/3].$$

This means vacancies will be located on every third (1, −1,2) plane when $x-y+2z=3p$ where p is an integer

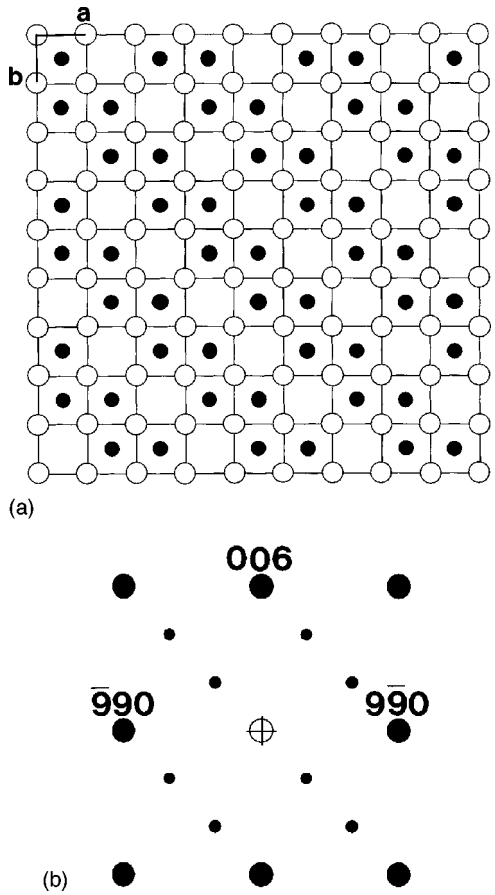

FIG. 10. (a) One plane ($z=0$) in the new (9**a**, 9**b**, 3**c**) cell showing the ordering of vacancies every third $(1,-1,2)$ plane. (b) Kinematical calculated diffraction pattern for this new structure, for a [110] zone axis. Note the superstructure spots, indexed in the (9**a**, 9**b**, 3**c**) cell.

$[n(x,y,z)$ is then equal to 0]. The structure is shown in Fig. 10(a) while the corresponding diffraction pattern is shown in Fig. 10(b). Note that we have ordered $\frac{1}{3}$ of the vacancies and that we are left with $\frac{4}{3}$ sites ($\frac{2}{3}$ of two possible sites) on which we still have to accommodate one vanadium atom.

Note also that we have to triple the a, b, and c parameters if we want to keep axes parallel to the bcc axes (volume of the new cell equal to 27 V_{bcc}): however, the symmetry is lowered, in particular the c axis is no longer a four-fold axis. As is obvious in Fig. 10(a) a smaller cell can be obtained by taking for translation vectors either $(\mathbf{a}-\mathbf{b})$ and $3(\mathbf{a}+\mathbf{b})$ (orthorhombic cell with a volume equal to 18 V) or $(\mathbf{a}-\mathbf{b})$ and $(\mathbf{a}+2\mathbf{b})$ (monoclinic cell with a volume of 9 V); for both cases, we keep $3\mathbf{c}$ as the third axis. Finally, let us remark that all (006) planes are equivalent as they are related by a translation of $(\mathbf{a}+\mathbf{b}+\mathbf{c})/2$.

We will investigate whether we can order vacancies in these planes. We can calculate the energy of our new compound and obtain

$$W' = 8X_1 \cos \pi k_x \cos \pi k_y \cos \pi k_z - 2X_1 \times \cos \pi(-k_x+k_y+k_z) + 2X_2(\cos 2\pi k_x + \cos 2\pi k_z) + 2X_3 \cos 2\pi k_y + 2X_4 \cos 2\pi(k_x-k_z).$$

Let us call $\mathbf{H}'$ a reciprocal lattice vector of the second ordering. We have to find a vector $\mathbf{k}'=\mathbf{H}'/n$ with $n=2$, 3, or 4, which minimizes W'. A minimum is obtained for the vector $\mathbf{k}_2'=1/3(1,1,2)$. This wave corresponds to a rather small decrease in energy: $W'(\frac{2}{3},\frac{2}{3},\frac{2}{3}) = -2X_2 - X_3 + 2X_4$ as can be expected for a ternary ordering. This last ordering with the vector $\mathbf{k}_2'$ would restore the tetragonal symmetry and lead to a structure $(V_{4/9}\square_{5/9})O$ and to $VO_2(A)$.[14]

However, as already pointed out by Khachaturyan,[13] our energy model is rather crude and we have to accept that other vectors, near the ones considered above, might give smaller or identical minima. However, these vectors will no longer be half, third, or fourth of host lattice reciprocal vectors. Following the procedure outlined in Ref. 13 we find that two possibilities can, indeed, provide a lower minimum: $\mathbf{k}_2=(2,1,9)/9$ for which the value of W' is $-4.76X_1 + 1.88X_2 + 2X_3 - X_4$; $\mathbf{k}_2''=(4,2,6)/9$ for which the value of W' is $-0.88X_1 - 1.53X_2 - X_3 + 0.35X_4$.

We now have dominant and secondary waves. If we take into account the fact that X_1 and X_2 are very similar (they correspond to interactions between atoms situated at nearly equal distances) and that the same holds for X_3 and X_4, we see that the energy variations are about the same. However, $\mathbf{k}_2$ exists in the reciprocal space of $VO_2(B)$ while $\mathbf{k}_2''$ does not. This $\mathbf{k}_2$ vector generates a layer structure perpendicular to $\mathbf{k}_2$. The proportion of vacant planes must be $n/9$, n being an integer. Since we want a stoichiometry as near as possible to $\frac{1}{2}$ we choose $n=3$. To deduce the sequence of full and vacant planes, we again use the clock diagram: the three vacant planes are sequential. We then obtain the structure shown in Fig. 11. For each plane perpendicular to c, one obtains the atomic arrangement of the $VO_2(B)$ structure. As in the previous paragraph one oxygen atom is not stable: hence, a vacancy will be created. The piling up of these planes along c, however, is no longer the same as in $VO_2(B)$ but gives rise to a very heterogeneous distribution and only small translations perpendicular to the c axis are needed to obtain the $VO_2(B)$ structure.

In summary, we can say that $VO_2(B)$ derives from a bcc lattice where vanadium atoms are introduced along with vacancies, on the octahedral interstices. Successive ordering of these vacancies can create stable structures that could form a homologous series. The successive orderings shown here lead to a formula V_4O_9 where one of the oxygen atoms is in an unstable position and will be replaced by a vacancy: all vanadium ions then have a valency $+4$.

IV. *IN SITU* ELECTRON MICROSCOPY STUDY OF $VO_2(B) \rightarrow VO_2(R)$

$VO_2(B)$ powder is crushed and mixed with alcohol before being dispersed on a Cu grid covered with holey carbon. Experiments are performed in a 120 kV or in a 200 kV electron microscope. The temperature of the heating holder is measured by a thermocouple, but the exact temperature of the crushed material is hard to determine accurately.

The initial powder mainly consists of thin and long platelike monocrystals with a monoclinic structure. The diffraction patterns are in good agreement with the $VO_2(B)$ structure determined by Théobald. $VO_2(B)$ platelets are mostly

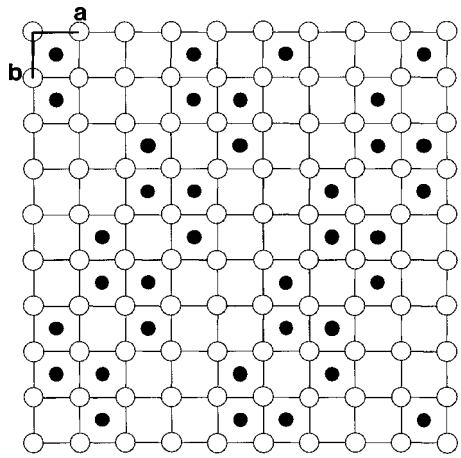

FIG. 11. One plane ($z=0$) in the new (9**a**, 9**b**, 3**c**) cell after two successive ordering. Vacancies are ordered every third $(1,-1,2)$ plane and packing of three sequential planes $\frac{1}{9}$ (2,1,9) out of 9 planes. This corresponds again, in one plane to the atomic arrangement of the $VO_2(B)$ structure.

oriented along $[001]_B$ or along a direction perpendicular to the (a,b) planes, which is $[106]_B$. In Fig. 12(a), we show the calculated diffraction pattern for the $[001]_B$ direction, while, in Fig. 12(b) we have calculated the diffraction pattern for a direction near the $[106]_B$ direction where we have taken into account some relaxation of the Bragg conditions due a size effect associated with defects (medium deviation to the Ewald sphere, $s=0.1$ Å^{-1}). The patterns differ in the intensity distribution of some spots but, geometrically, they are identical. Figure 12(c) shows the experimental diffraction pattern. This will be our starting orientation for the heating experiment, the electron beam being roughly perpendicular to the (a,b) plane. On the low *magnification* images of Fig. 13(a), a number of planar defects are present; their origin is clear from high-resolution electron microscopy images such as Fig. 13(b). They are identified as twin interfaces with the twin plane being the (100) plane. The zero-order Laue zone of the $[001]_B$ section is insensitive to twinning but the $[106]_B$ is not, which explains why we can see the effect of the twinning, as a slight difference in background contrast. This confirms, if needed, that the electron beam is not exactly along the [001] direction.

During heating, we observe a strong change in the *microstructure* of the platelike monocrystals associated with important modifications of the diffraction patterns.

The first change in reciprocal space is the vanishing, around 200 °C, of most of the long-range order reflections such as 200 and 400 [Fig. 14(a)]; only the 601 (or 600), 020- and 110-type reflections maintain their intensity. At a later stage the 110 reflections also strongly decrease in intensity. This implies that the long-range order of the octahedra (Fig. 8) is mostly destroyed. In order to explain the vanishing of the superstructure reflections one has to assume a breaking of the interconnections between different octahedra, which are either corner sharing or edge sharing in the $VO_2(B)$ structure.

As the $VO_2(B)$ reflections disappear, other reflections appear, mainly associated with the reflections 601_B and 020_B; they are indicated by X and Y in Fig. 14(b); at first sight, the X spots look more like satellites and do not form a superstructure while the Y spots are regularly aligned between bcc-type spots. Note that fourfold symmetry is not restored and that the splitting is asymmetrical. This X structure, however, is restricted to nanosize domains and can be shown to correspond to symmetric orientations of a monoclinic intermediate structure with an angle slightly different from 90°.

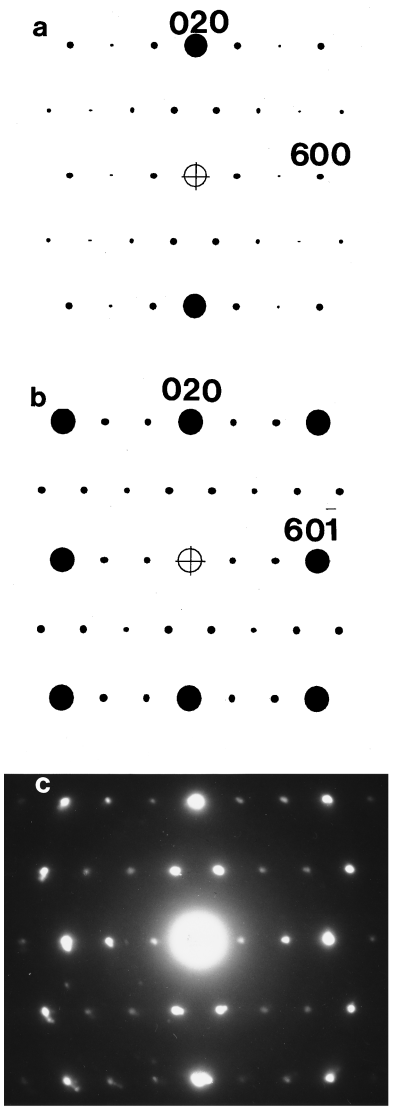

FIG. 12. Diffraction patterns for the $VO_2(B)$ structure. (a) Calculated diffraction pattern for a [001] zone axis. (b) Calculated diffraction pattern for a [106] zone axis, with $\Delta s=0.1$ Å^{-1}. (c) Experimental diffraction pattern.

The other reflections in Fig. 14(b), marked Y, cannot be explained on the basis of this monoclinic distortion; they must have a different origin. Upon careful further heating (not passing the rutile transition) one can see the X-type reflections vanish [Fig. 14(c)] while the Y reflections develop to form a true superstructure [see Fig. 14(d)]. This pseudotetragonal diffraction pattern clearly consists of two orientation variants, rotated 90° with respect to each other. This is, e.g., evident in the initial stages in Fig. 14(b) where one variant is much stronger than the other. The diffraction patterns shown in Figs. 14(b) and 14(d) can be compared to the calculated diffraction pattern Fig. 11 obtained in Sec. III.

In real space, one can follow the morphology of the platelets during the heating experiment. The platelet shape is

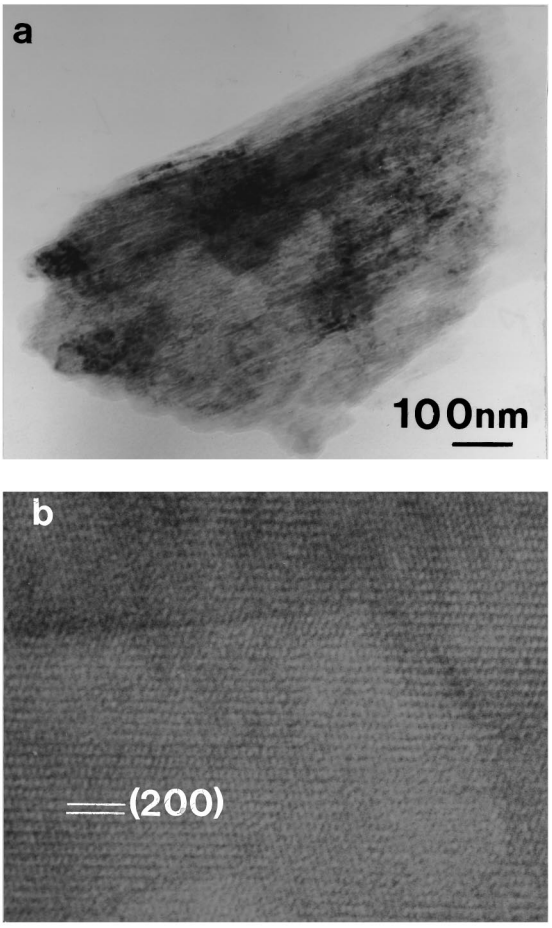

FIG. 13. (a) Low magnification image of one $VO_2(B)$ platelet. (b) lattice fringes image showing the (1,1,0), the $(-1,1,0)$, and the (2,0,0) planes.

maintained as long as one does not reach the temperature where the rutile phase is formed. Fig. 15(a) shows the same platelet as in Fig. 13(a), but at a temperature near the transition temperature; the corresponding diffraction pattern is shown Fig. 14(c). Although the shape of the platelet remains, it consists now of two types of domains, roughly oriented perpendicular to each other, and at 45° of the twins interfaces existing in the initial $VO_2(B)$ platelet.

Upon continued heating, the platelets abruptly break up into nanocrystallites and recrystallize into the rutile structure [Fig. 15(b)]. Such breaking up is clearly necessary in view of the completely different arrangement of the VO_6 octahedra in both structures. No orientation relationship exists between the phase $VO_2(B)$ and the rutile phase, nor between neighboring rutile type grains. Remarkably, no oxygen is lost during this complete transformation cycle, although the morphology and the shape of the crystal does change drastically during the transition.

V. DISCUSSION AND CONCLUSION

The phase transition from $VO_2(B)$ to $VO_2(R)$ is remarkable and very unusual. While $VO_2(B)$ as well as $VO_2(A)$ and all related structures- is based on an ordered arrangement of single axis aligned octahedra, the rutile form of VO_2 is built up from octahedra aligned along two mutually perpen-

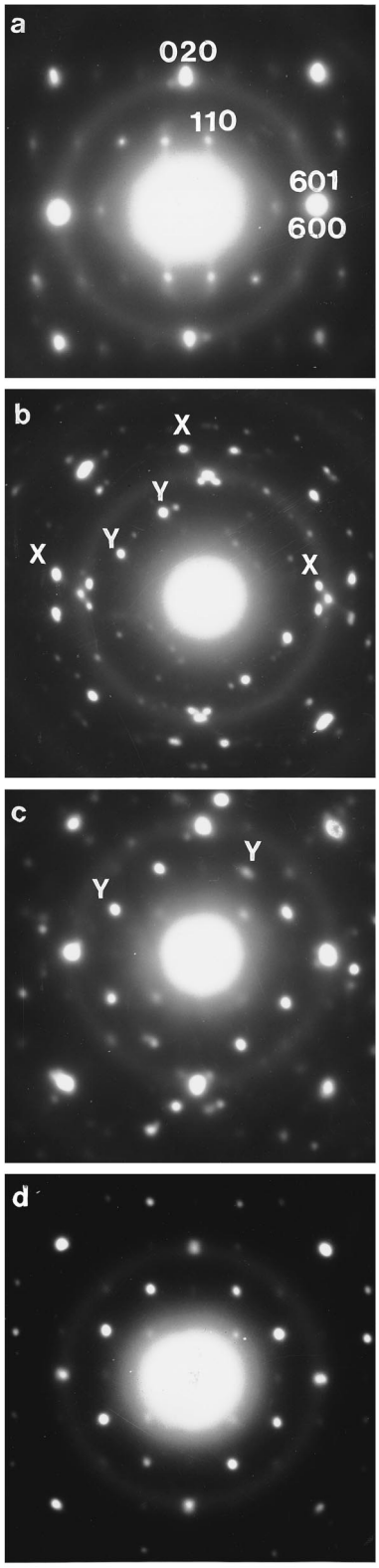

FIG. 14. Evolution of the diffraction patterns during the heating experiment. (a) first stage; disappearance of spots characteristic of the $VO_2(B)$ structure, (b) second stage; new spots appear, (c) third stage; disappearance of spots marked X, (d) final stage before the formation of $VO_2(R)$ crystals; diffraction pattern with a tetragonal symmetry.

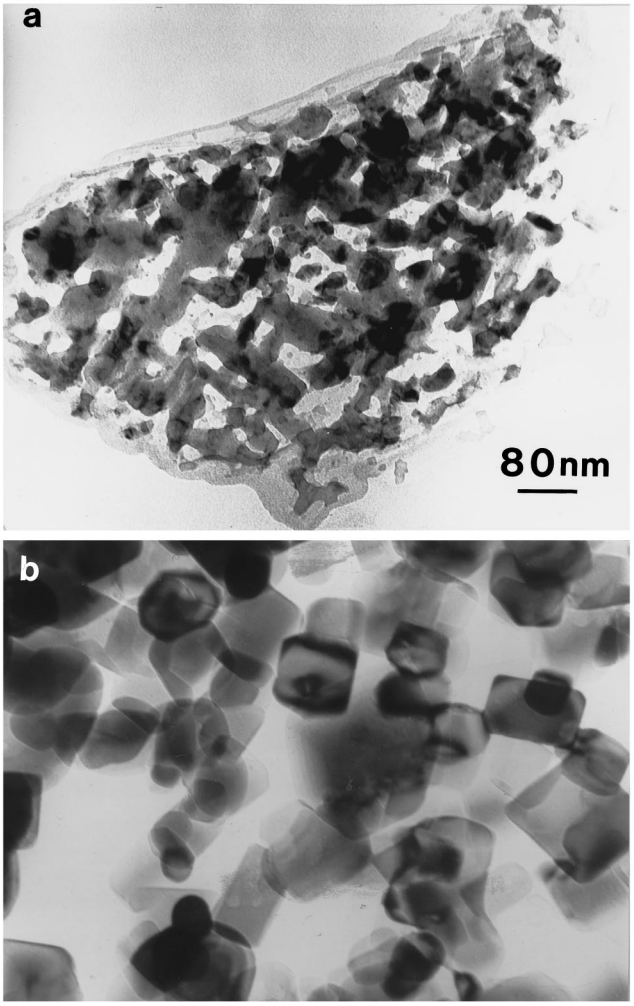

FIG. 15. Evolution of the morphology of the platelets. (a) Image of a platelet, taken just before the transformation into crystallites of $VO_2(R)$ occurs. (b) Final crystallites of $VO_2(R)$.

dicular *directions*. However before the octahedra more or less break apart and order themselves along two perpendicular axes, a lot of rearrangement and reshufling has taken place within the structure. This is the first time these changes have been carefully recorded and their structure analysed. The fact that this transition has been studied inside the vacuum of the electron microscope under an electron irradiation of 120 kV or *higher* might raise the question on the intrinsic character of this transition. However, the differential scanning calorimetry measurements show that the transition is not a simple one and occurs at least in two steps.

A question which has puzzled a number of scientists is the occurrence of the $VO_2(A)$ phase during the transition. The presence of this phase was proposed by Theobald[3] and later by Oka, Yao, and Yamamoto.[4] We have no evidence for the presence of $VO_2(A)$ at any stage during the transformation; the strongest reflections of $VO_2(B)$ (020 and 600) are very close to the stronger reflections of $VO_2(A)$ (330 and 004), as they all are in fact reflections corresponding to the bcc lattice (see Sec. III). The theoretical considerations in Sec. III indicate that $VO_2(B)$ and $VO_2(A)$ have a common first ordering of vanadium vacancies [due to a dominant wave $\frac{1}{3}$ (1, -1,2)] but the second ordering is different. Our heating experiments can be interpreted in the following way: by heating up the $VO_2(B)$, this structure changes into a structure of higher symmetry, more stable from a thermodynamical point of view, the parent phase, generated by the SCW $\frac{1}{3}$ (1, -1,2). This change includes a translation of the planes perpendicular to the bcc c axis, back to their position in the parent phase, giving rise to an intermediate structure with an angle different from 90°. At this stage, the distinction between $VO_2(B)$ and $VO_2(A)$ becomes irrelevant as they both have the same parent structure. Further heating disorders even more the vacancies and the vanadium atoms on the octahedral sites. When complete disorder is reached, the crystal assumes the more stable rutile structure.

As a summary, we have shown theoretically that the structures of the VO_2 polymorphs $VO_2(B)$ and $VO_2(A)$ correspond to different orderings of vanadium atoms on the octahedral sites of a bcc oxygen lattice, like the well-known $VO_2(R)$. $VO_2(B)$ and $VO_2(A)$ have an ordering of vanadium atoms on only one octahedral sites sublattice. The stable structure $VO_2(R)$ presents an ordering of vanadiums on two different octahedral sites sublattices. This explains why the final step of the transformation from $VO_2(B)$ into $VO_2(R)$ is a reconstructive one. Experimentally, the in situ electron microscopy study has also shown the different stages of the $VO_2(B) \rightarrow VO_2(R)$ transition. Our theoretical considerations explain the evolution from $VO_2(B)$ into an intermediate phase of higher symmetry, before the final reconstructive transformation.

ACKNOWLEDGMENTS

It is a pleasure to thank J.-Ch. Valmalette, MMI, University of Toulon, for providing the $VO_2(B)$ powders, and Veronique Buschmann, IUAP IV-10, for her assistance during the heating experiments at EMAT in Antwerp.

[1] J. C. Valmalette and J. R. Gavarri, Sol. Energy Mater. Sol. Cells **33**, 135 (1994).
[2] J. C. Valmalette and J. R. Gavarri, Eur. J. Solid State Inorg. Chem. (to be published).
[3] F. Theobald, J. Less-Common Met. **53**, 55 (1977).
[4] Y. Oka, T. Yao, and N. Yamamoto, J. Mater. Chem. **1**, 5 (1991).
[5] Y. Oka, T. Yao, and N. Yamamoto, J. Solid State Chem. **86**, 116 (1990).
[6] G. Anderson, Acta Chem. Scand. **10**, 623 (1956).
[7] A. D. Burton and P. A. Cox, Philos. Mag. B **51**, 2 (1985).
[8] J. M. Longo and P. Kierkegaard, Acta Chem. Scand. **24**, 420 (1970).
[9] J. C. Rakotoniaina, R. Mokrani-Tamellin, J. R. Gavarri, G. Vacquier, A. Casalot, and G. Galvarin, J. Solid State Chem. **103**, 81 (1993).
[10] F. Theobald, R. Cabala, and J. Bernard, J. Solid State Chem. **17**,

431 (1976).
[11] A. G. Khachaturyan and B. I. Pokrovskii, Prog. Mater. Sci. **29**, 17 (1985).
[12] B. I. Pokrovskii and A. G. Khachaturyan, J. Solid State Chem. **61**, 137 (1986).
[13] B. I. Pokrovskii and A. G. Khachaturyan, J. Solid State Chem. **61**, 154 (1986).
[14] C. Cesari, Ch. Leroux, and G. Nihoul (unpublished).